OPEN ACCESS
IOP Publishing
Journal of Physics B: Atomic, Molecular and Optical Physics
J. Phys. B: At. Mol. Opt. Phys. **53** (2020) 092001 (20pp)
https://doi.org/10.1088/1361-6455/ab69aa

Roadmap

Roadmap on cosmic EUV and x-ray spectroscopy

Randall Smith[1,13], Michael Hahn[2], John Raymond[1], T Kallman[3], C P Ballance[4], Vanessa Polito[5], Giulio Del Zanna[6], Liyi Gu[7], Natalie Hell[8], Renata Cumbee[3], Gabriele Betancourt-Martinez[9,10], Elisa Costantini[11] and Lia Corrales[12]

[1] Center for Astrophysics, Harvard & Smithsonian, Cambridge, MA 02138, United States of America
[2] Columbia Astrophysics Laboratory, Columbia University, NY 10027, United States of America
[3] NASA Goddard Space Flight Center, Greenbelt, MD 20771, United States of America
[4] CTAMOP, Old Physics Building, Queen's University of Belfast, Belfast, BT7 1NNN, United Kingdom
[5] Bay Area Environmental Research Institute, Lockheed Martin Solar and Astrophysics Laboratory, 3176 Porter Dr, Palo Alto, CA 94304, United States of America
[6] Department of Applied Maths and Theoretical Physics, University of Cambridge, Cambridge CB3 8WA, United Kingdom
[7] High Energy Astrophysics Laboratory, RIKEN, 2-1 Hirosawa, Wako, Saitama 351-0198, Japan
[8] Lawrence Livermore National Laboratory, Livermore, CA 94550, United States of America
[9] The Research Institute in Astrophysics and Planetology, F-31400 Toulouse, France
[10] CNRS, F-75016 Paris, France
[11] SRON Netherlands Institute for Space Research, Sorbonnelaan 2, 3584CA, Utrecht, The Netherlands
[12] Astronomy Department, University of Michigan, Ann Arbor MI 48014, United States of America

Received 23 October 2019, revised 20 December 2019
Accepted for publication 9 January 2020
Published 6 April 2020

Abstract

Cosmic EUV/x-ray spectroscopists, including both solar and astrophysical analysts, have a wide range of high-resolution and high-sensitivity tools in use and a number of new facilities in development for launch. As this bandpass requires placing the spectrometer beyond the Earth's atmosphere, each mission represents a major investment by a national space agency such as NASA, ESA, or JAXA, and more typically a collaboration between two or three. In general justifying new mission requires an improvement in capabilities of at least an order of magnitude, but the sensitivity of these existing missions are already taxing existing atomic data quantity and accuracy. This roadmap reviews the existing missions, showing how in a number of areas atomic data limits the science that can be performed. The missions that will be launched in the coming Decade will without doubt require both more and improved measurements of wavelengths and rates, along with theoretical calculations of collisional and radiative cross sections for a wide range of processes.

Keywords: cosmic EUV, x-ray spectroscopy, astrophysics, atomic data

(Some figures may appear in colour only in the online journal)

[13] Guest editor of the Roadmap.

Contents

1. Introduction

Randall Smith

Center for Astrophysics|Harvard & Smithsonian

Cosmic x-ray and EUV spectroscopy has entered a Golden Era, with a wide range of high-resolution spectrometers observing the Sun, the solar system, and distant astrophysical sources as well as new facilities in development for launch. Table 1 shows a list of all missions either in current use or fully funded, covering the entire x-ray/EUV bandpass. As this bandpass requires placing the spectrometer beyond the Earth's atmosphere, each mission represents a major investment by NASA, ESA, or JAXA—typically requiring at least an order of magnitude improvement over previous missions. As described in this roadmap, the sensitivity of existing cosmic spectrometers are already revealing the limits of existing atomic data. The missions that will be launched in the coming decade will require improved measurements of wavelengths and rates, along with theoretical calculations of collisional and radiative cross sections for a wide range of processes.

Understanding cosmic spectroscopic observations requires plasma models to describe the spectrum, which in turn require a range of Atomic, Molecular, and Optical (AMO) data. The multiple scientific areas involved—observational, theoretical, and instrumental—create challenges for anyone attempting a brief review. We have chosen to focus on the AMO data as an organizing principle, rather than plasma models or types of cosmic sources. Section 3 (Hahn and Raymond) describes the electronic collisional ionization and recombination rates required to calculate the charge state distribution (CSD) of a collision-dominated plasma, such as occurs in the solar corona, galaxy cluster, or supernova remnant. Section 5 (Kallman and Ballance) reviews the photoionization and photo-excitation rates necessary to determine the CSD of a radiation-dominated plasma, which may be found near an accreting black hole or other compact source. Section 6 (Polito and Del Zanna) covers primarily transitions in the EUV, with a particular focus on solar observations. This latter focus arises as solar missions often rely upon EUV diagnostics, while astrophysical missions avoid them due to the limitations created by interstellar gas and dust absorbing distant EUV.

In section 8, Gu and Hell review the status of x-ray transitions, concentrating on astrophysical plasma needs and recent results. The final two sections describe AMO interactions in space whose diagnostic power has only begun to be explored. Section 10 (Cumbee and Betancourt-Martinez) describes the status of calculations and measurements of charge exchange interactions. This process is known to occur within the solar system, for example, as x-rays are emitted after the highly-ionized solar wind interacts with neutral material in and around comets. Recent observations have suggested charge exchange can also be found in supernova remnants, starburst galaxy outflows, and the centers of galaxy clusters but in general current observatories lack the sensitivity to make unambiguous detections. The next generation of astrophysical observatories, however, will be able to detect and quantify emission due to charge exchange, so the time is right to improve both laboratory measurements and theoretical calculations. Finally, section 12 (Costantini and Corrales) describes interactions with solid state materials such as dust grains in the interstellar medium. As with charge exchange, existing observations can detect some features but cannot conclusively identify the chemical composition of various materials. Missions such as x-ray imaging and spectroscopy mission (XRISM) and Athena, however, should be able to use x-ray absorption fine structure (XAFS) and x-ray absorption near-edge structure features to determine grain compositions directly, a long-awaited capability.

Table 1. Existing and approved spectroscopy missions in the EUV/x-ray bands. Typical resolutions are in the range of $\lambda/\Delta\lambda = 300$–$8000$, higher in the EUV and lower in the x-rays.

	Mission	Bandpass (nm)	Status
Astro	Chandra/HETG	0.12–31	In orbit
	Chandra/LETG	0.12–17.7	In orbit
	XMM-Newton/RGS	0.5–3.5	In orbit
	XRISM/Resolve	0.1–4.1	2022 launch
	Athena/X-IFU	0.1–6.2	2031 launch
Helio	Hinode EIS	17–21.1	In orbit
		24.5–29.2	In orbit
	SDO EVE	17–105	In orbit
	IRIS	133.2–135.8	In orbit
		138.9–140.7	In orbit
		278.3–283.4	In orbit
	EUNIS-2	8.9–11.2	2019 launch
		52–64	2019 launch
	Solar Orbiter/	70.4–79	2020 launch
	SPICE	97.3–104.9	2020 launch
	MaGIXS	0.6–2.4	2020 launch

Current and future challenges. Prior to the launches of Chandra and XMM-Newton in 1999, the x-ray astrophysical community was aware that existing plasma models had to be improved as they either lacked or had inadequate data for a number of significant ions (in particular Fe L and Fe M shell ions). This problem was solved thanks to a combination of consistent effort from the AMO community (both experimental and theoretical), aided by significant advances in computing capability.

The capabilities of the next missions will open a new frontier for analysts. In general, EUV/x-ray spectroscopy of cosmic sources has been analyzed assuming the underlying AMO data are perfect—that wavelengths are accurate, CSDs are exact down to relative abundances of 0.01%, and diagnostic ratios of emission lines are error-free. While the analysts realize this is not the case, they have had little choice but to work with this assumption. The substantial effort required to propagate either measurement errors from laboratory data or estimates of the (correlated!) theoretical uncertainties into plasma models was generally not feasible. Even in those cases where this can be done, cosmic spectral

analysis tools do not include any facility for including uncertainties from the plasma model (as opposed to the observed spectra itself) in their results. Breaking these assumptions will require a concerted effort by AMO experimentalists and theorists as well as those developing plasma models and analysis tools.

Of course, there will always be errors, uncertainties, or limitations in all atomic data, both laboratory measurements and theoretical calculations. The relevant question is whether or not these atomic data errors dominate, match, or are smaller than the other systematic and statistical errors in the data. Of particular concern is if the atomic data errors drive the derived physical parameters—e.g. wavelength errors leading to incorrect Doppler shifts or excitation rate uncertainties causing derived abundance errors. As described in the following sections, the measurement accuracies needed for each rate or value is therefore not an absolute, but depends upon the observatory's capabilities, the astronomical sources being observed, and the parameters being derived.

Acknowledgments

The author thanks Jelle Kaastra, Adam Foster, and Nancy Brickhouse for stimulating discussions, and acknowledges support for this work from NASA grant #80NSSC18K0409.

2. Collisional ionization and recombination

Michael Hahn[1] *and John Raymond*[2]

[1]Columbia University [2]Center for Astrophysics|Harvard & Smithsonian

Status. Collisional ionization and recombination data are needed to determine the CSD and diagnostic emission and absorption line strengths in optically thin plasmas throughout the universe. Some examples include the coronae of the Sun and other stars, shock waves in supernova remnants, jets from young stars, hot gas in clusters of galaxies, H II regions, galaxy halos, planetary nebulae, active galactic nuclei (AGN), and accretion disk coronae in x-ray binaries. These data are needed for the cosmically abundant elements hydrogen through zinc. Because of the large number of systems, most are generated by theoretical calculations.

The reaction cross sections depend on the collision energy or, equivalently, the velocity. Since the electrons in a plasma have a distribution of velocities, the collision data are usually reported as a reaction rate coefficient, α, that is the cross section multiplied by the velocity and averaged over the distribution. The distribution is most often taken to be Maxwellian and so $\alpha(T)$ is a function of temperature. For collisionally ionized plasmas, the electron temperature in energy units, kT, is about $1/4$ of the ionization threshold for the abundant ions whereas in photoionized plasmas kT is typically a few percent of the ionization potential of the most abundant charge states.

In addition to providing a temperature diagnostic, the CSD also influences other measurements. Elemental abundances are found from the line strengths of different species normalized by their ionization fractions. Densities are determined from the ionization states of photoionized plasmas or from the rate of change of the ionization state. Physical processes, such as heating rates, can be derived from these parameters.

Collisionally ionized plasmas are produced by electron impact ionization (EII). EII may be divided into direct and indirect processes [1]. Direct ionization occurs when an incoming electron knocks an electron off the target ion. Indirect ionization occurs when the electron–ion collision excites the target ion to a level that decays by ejecting an electron. Such indirect processes include excitation-autoionization (EA), resonant excitation double-autoionization and resonant excitation auto-double-ionization [1]. Of the indirect processes, EA has the largest influence on the total cross section and the plasma CSD.

Recent compilations of EII data have been given by [2, 3]. In those works, empirical results were used where possible and supplemented by calculations for the unmeasured systems. Another useful database for EII cross sections is maintained by the National Institute for Fusion Science in Japan (https://dbshino.nifs.ac.jp/nifsdb/). Recent experiments have revealed several shortcomings of earlier EII data

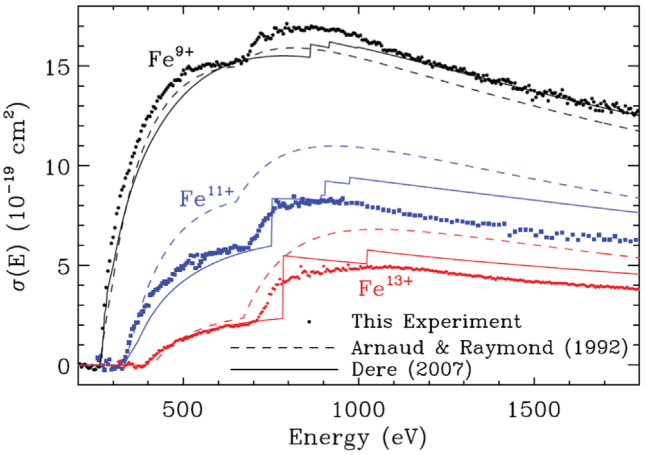

Figure 1. EII cross sections for several iron ions comparing results from storage ring experiments [5] (filled points) to the recent compilation of Dere [2] (solid curve) and the earlier recommended cross sections of Arnaud and Raymond [88] (dashed curves). Reproduced from [88]. © IOP Publishing Ltd. CC BY 3.0.

(figure 1). First, cross sections are usually reported for ionization from the ground state, but much of the earlier experimental data came from crossed beams experiments in which an unknown fraction of the measured ions were in metastable excited states. Recent storage ring experiments overcame this limitation by storing the ions long enough for the metastables to decay before measuring the EII cross sections. Those measurements have found that for ions affected by metastable contamination the EII cross sections from the ground state are significantly smaller (∼40%) than reported earlier [5]. The storage ring work also showed that theory systematically overestimates the cross sections for some EA channels.

Radiative recombination (RR) and dielectronic recombination (DR) are the most important recombination processes, with DR usually dominant [1]. RR occurs when an ion captures an electron by emitting a photon. DR is a resonant process in which the capture of the free electron is accompanied by an excitation of a bound electron forming a doubly excited state. If the excited ion decays radiatively, then the recombination is complete. Conversely, the excited state may decay by autoionization, resulting in no net change in the ion's charge state. The resonant energies for DR form a Rydberg series that depend on the excitation energies for the core electrons. The amplitudes of the DR cross sections depend on the relative probability of radiative decay versus autoionization of the intermediate state.

Many calculations for RR and DR have been performed and the data can be accessed through compilations such as CHIANTI or the Atomic Data and Analysis Structure (http://open.adas.ac.uk). For low density plasmas, total recombination cross sections are sufficient, but for DR at high densities collisions can ionize the intermediate states or redistribute their populations and so level-resolved data are needed. Such data are also needed to interpret spectra, such as from planetary nebulae and H II regions, where recombination

produces optical and UV lines that imply different elemental abundances than do the collisionally excited lines [6]. Some level-resolved data have been calculated using the AUTOSTRUCTURE code [7].

Most recent experimental measurements for DR have been performed at storage rings [8]. Those experiments revealed inaccuracies in the previously available DR data due to difficulty calculating the low energy DR resonances. Interaction between experiment and theory has led to significant improvements so that total DR rate coefficients from state-of-the-art theories typically agree with measurements to $\sim$30%.

Current and future challenges. The Hitomi Collaboration [60] found that differences in atomic data were amongst the largest systematic uncertainties in measurements of flux, temperature, and abundances for the Perseus cluster, the one source with a robust observation. As new x-ray observatories are launched in the next decade, we must both better understand these uncertainties and reduce their impact. One objective for ionization and recombination is to reduce uncertainties to less than 10%. While that level of accuracy is attained for simple isoelectronic sequences (e.g. H- and He-like ions), the uncertainties for most ions are at least twice as large. More data for state-specific recombination are needed. Cross sections for ionization and recombination from metastable levels are also needed for ions with significant metastable populations, e.g. Be- and Mg-like. State specific data and data for metastable levels in particular are especially important for denser plasmas, for example, where the ionization balance can become density-dependent [9].

Modern high resolution, high signal-to-noise ratio spectra need data for heavier elements. This poses a challenge as such ions exhibit more complex processes. For example, storage ring measurements, motivated by fusion plasma applications, have shown that DR for complex ions (e.g. W^{20+}, Au^{25+} [8]) are orders of magnitude larger than predicted. In order to accurately model this DR, theory has resorted to a statistical description to account for the strong mixing of many closely spaced resonance levels. Even more exotic processes are possible. For example, low charge states of heavy ions may exhibit polarization recombination in which polarization of the target ion by the incident electron causes the emission of a photon and that allows the electron to be captured [10]. Likewise, ionization of heavy ions becomes more complicated due to the increasing contribution of indirect processes.

Multiple ionization may be important for dynamic plasmas or non-thermal plasmas with a large population of high energy electrons. In multiple ionization a single electron–ion collision leads to the ejection of more than one electron. Predicting these cross sections involves a multi-body collision problem. Consequently, quantum mechanical calculations are limited and most data come from extrapolations of experimental results using semi-empirical trends with large uncertainties [11].

Increasing interest in non-thermal plasmas creates a need for appropriate atomic data. Raw cross section data can be complex, for example DR cross sections have a dense resonance structure. Averaging the data over an energy distribution smooths out these structures and results in an α (T) that can be parameterized with a few coefficients. As a result, most databases for astrophysics contain only the Maxwellian-averaged rate coefficients rather than the cumbersome cross section data. In order to adapt the Maxwellian data to use for non-thermal plasmas, methods have been developed to reverse engineer the cross section data from the tabulated Maxwellian rate coefficients or to decompose the non-thermal distributions into a sum of Maxwellians [12]. It would be more accurate to tabulate the cross section data so that it could be convolved with any needed distribution. This poses a practical challenge for databases.

Finally, observers have long recognized the importance of understanding the uncertainties associated with atomic data. However, theoretical calculations typically do not generate uncertainties on their predictions. Some effort has been made in estimating the theoretical uncertainties so that these error bars can be propagated into spectroscopic analysis [4], but more work is needed and it is still far from the norm to include such uncertainty estimates for theoretical data.

Advances in science and technology to meet challenges. Increasing the accuracy of the atomic data will require a more comprehensive inclusion of reaction pathways in the calculations. For example, EII experiments have found discrepancies with the theoretical calculations for EA because some channels were ignored. Recent experiments have found that for some ions an important recombination process is trielectronic recombination (TR), in which a resonant capture occurs through the double-excitation of the target ion that forms a triply excited intermediate state. Modern theories can calculate the TR contribution if those channels are considered in the model. As more infrared observations become available, it is also important to extend the recombination rate measurements to very low temperatures, which requires increasing the precision of the data for the low energy resonances. Extending the atomic dataset for astrophysics to heavier ions will add increasing complexity.

Interaction between theory and experiment will remain important. Experimental measurements are needed to benchmark calculations, especially for systems and processes that are most challenging for theory, such as heavy ions and multiple ionization.

Concluding remarks. Collisional ionization and recombination data are needed to interpret spectra from a broad range of astrophysical objects. Improvements over the last decade have greatly improved the accuracy of these data. Future work will likely focus on further improvements to precision,

extending the dataset to heavier elements, obtaining state-resolved collision data, and accounting for more exotic processes. These results will form the foundation for future advances in astrophysics.

Acknowledgments

The authors thank Daniel Wolf Savin for stimulating discussions. MH acknowledges support from NSF and NASA.

3. Photoabsorption and photoionization

T Kallman[1] and C P Ballance[2]

[1]NASA's GSFC [2]CTAMOP

Absorption in atomic bound-bound or bound-free transitions is of universal importance in x-ray astronomy. It occurs most obviously in the photoelectric absorption associated with intervening material along the line of sight to a distant x-ray source. Often the source is the principle object of interest, and absorption is treated as a by-product. When the intervening material is of interest, the absorption can be used to derive element abundances and to search for molecules or solids. In sources containing an intense source of continuum x-rays and associated cooler gas, such as accreting black holes and neutron stars, photoionization can be the dominant mechanism affecting the ionization, excitation and temperature; modeling of these processes can allow study of the continuum source and the associated gas. In all of these contexts, knowledge of photoabsorption and photoionization cross sections are needed to advance scientific study.

The cross section for bound-free photoionization has a characteristic behavior which is a sharp threshold determined by energetics, a near-threshold cross section $\sim\pi(a_0/z)^2$ where a_0 is the Bohr radius and z is the nuclear charge, and a decrease with energy $\propto E^{-3}$ at higher energies. In a neutral cosmic gas with typical elemental abundances all the elements conspire to produce a cross section which is $\sim 2.5\times10^{-22}\ E_{\rm KeV}^{-3}$ cm^2 where $E_{\rm KeV}$ is the photon energy in keV [13]. Typical interstellar column densities are $\geqslant 10^{20}$ cm^{-2} so that absorption becomes important at some energy greater than $\sim$0.2 keV. Little information is contained in the smooth part of the interstellar absorption spectrum, but abundant trace elements such as O, Ne and Si imprint the energy jump at threshold onto the spectrum. These features allow measurement of the abundances of these elements [14]. It is also important to have accurate cross sections for the interstellar absorption in order to obtain the intrinsic spectrum of the distant source. Considerable effort has been devoted to this, leading to public code packages which allow varying elemental abundances and dust composition to be fitted [15].

At a more detailed level, the interstellar absorption contains information about the kinematics and elemental composition and also about the chemical binding of the constituent elements. This comes from the strength and structure of the K lines, and their energies or Doppler shifts [16]. It requires laboratory spectra of x-ray absorption from atoms, ions, molecules and solids. Efforts to measure and collect such data are ongoing [17]. It is important to note that the data needed for this effort go beyond line energies and oscillator strengths of cross sections. Most K lines are damped by Auger decay, and the transition probability for this process is needed for accurate application to astrophysical measurements.

For situations where intense continuum x-rays dominate the ionization and heating, we model the population kinetics and temperature by assuming a balance between the photoionization and recombination, between photoexcitation in bound-bound transitions and spontaneous decay, and between heating by photoelectrons (or Compton scattering) and cooling by emission of radiation. The general problem of calculating the reprocessing of ionizing continuum radiation from a star or compact object into longer wavelength lines and diffuse continuum has broad importance in astrophysics. Typical photoionization models calculate the ionization, excitation, and heating of cosmic gas by an external source of photons. The gas is generally assumed to be in a time-steady balance between ionization and recombination, and between heating and cooling. Such modeling requires an extensive library of photoionization cross sections for many ions and their bound levels. Current state of the art data can come from detailed *R*-matrix calculations, described in the following section.

A more detailed summary beyond that described here would require a dedicated paper but many areas of progress have been described by [18–20]. Notable are the measurements carried out using merged beams at the advanced light source, Berkeley and elsewhere [21]; ongoing measurements by electron beam ion traps (EBITs) [22]; and synchrotrons in Germany [23] and France [24].

Theory. The photoionization and photo-absorption of atoms and ions [25] has been a topic of theoretical interest for many decades. Theoretical approaches to photoionization/photoabsorption include perturbative distorted-wave methods as implemented within modern codes such as FAC [26] and AUTOSTRUCTURE [27]. Non-perturbative methods include the convergent-close coupling [28], time-dependent close-coupling [29] and *R*-matrix [30] approaches. Traditionally the non-perturbative methods were more computationally intensive and therefore time-consuming relative to their perturbative counterparts. In particular the *R*-matrix codes were structured to provide detailed comparisons with high resolution measurements rather than effectively providing the comprehensive coverage of bound-bound, bound-free and free-free transitions that constitute a Rosseland-mean opacity.

Of the non-perturbative methods, *R*-matrix theory has the strengths that it naturally includes photoionization, photo-excitation and all the Rydberg resonance structure inherently within the method and through current message passing interface (MPI) parallelism can provide highly delineated cross sections with millions of photon energy points. The ability of the parallel DARC code [31] to reproduce the high resolution experimental measurements for most of the periodic table [32–34] is well-documented. However, there are a couple of emerging issues to address.

For inner-shell soft x-ray photoionization, as the incoming photon can span thousands of Rydbergs, the size of both the Hamiltonian matrices and the dipole matrix files grow in size. Ideally, we would like to treat valence shell, as well as K, L, M shell photoionization in a single calculation, but this may be beyond current computational limits. However,

progress has been made and is described in the subsequent paragraphs.

Secondly, stellar opacities require an order of magnitude more photoionization cross sections, specifically the photoionization from all excited states, not just the groundstate and first few metastables. Figure 2 shows the photoionisation of every initial level of Fe XVII up to configurations involving $n = 5$ orbitals. Both the valence shell electron and 2s electron may be directly photoionised. As the initial states increase in n shell, the direct ionization limit decreases in terms of energy, and therefore the 2s ionisation threshold marches downwards in energy. The graph illustrates the level of completeness required for a Rosseland Mean opacity. To address these issues, the parallel R-matrix codes have been refactored to concurrently calculate every dipole matrix required simultaneously, reducing the total time required to the generation of largest dipole matrix. The current version of the code is flexible enough to assign different number of processors to the construction of each dipole matrix based upon the size and hence the computational effort required to construct it. The diagonalization of every Hamiltonian is again carried out concurrently on an arbitrary number of processors of the users choosing. The last remaining obstacle for both soft x-ray photoionization and for stellar opacities is the formation of the dipole matrix. In matrix notation, the dipole matrix excluding any outer region contributions is given by equation (51) of [35].

$$D(a, b) = F^T{}_a R_a^{-1}\, w_a G_a M(a, b)\, G_b w_b R_b^{-1}\, F_b, \qquad (1)$$

where if a is an initial discrete state with known quantum numbers and b a continuum state with dipole allowed quantum numbers with respect to a. $F^T{}_a$ is a matrix representing discrete negative energy boundstate wavefunctions and F_b is a matrix representing continuum states. $R^{-1}{}_{a,b}$ represents the inverse of the R-matrix for symmetries a, b, $w_{a,b}$ are the surface amplitudes for symmetries a, b. $G_{a,b} = 1/(2r_a)\ (E_k - E)^{-1}$ where E_k corresponds to the eigenvalues of the Hamiltonian representing either symmetry a or b, and r_a the size of the R-matrix box. The matrix M is the product of one-electron matrix elements and the eigenvectors corresponding to symmetry a and b, given by the following expression

$$M(a, b) = V^T{}_a M\ V_b. \qquad (2)$$

As the Hamiltonian matrices exceed 100 000 by 100 000, as do the associated eigenvectors $V_{a,b}$, being the same size. As matrix multiplication is an n^3 process, equation (2) can quickly exceed $10^{15,16}$ operations with current processor CPU speeds typically of the order 10^9 flops. MPI parallelism can mitigate the problem by slicing the matrix-multiplication over a number of processors but it is the advent of graphical processing units (GPU) that have dramatically impacted the solution. GPUs allow the dense matrix multiplies to be off-loaded from the CPU to the GPU with an associated speed-up

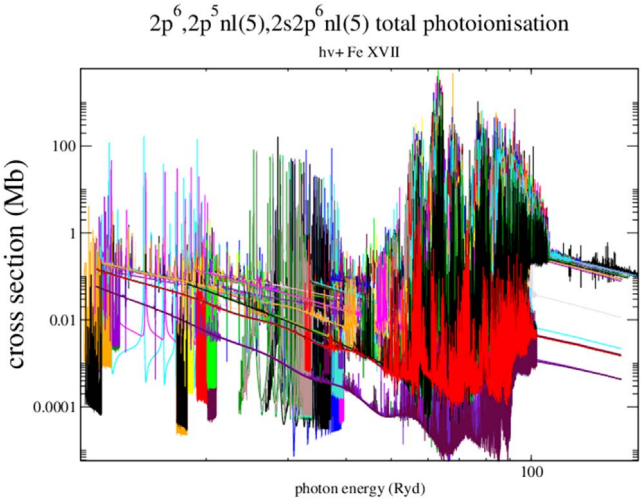

Figure 2. An R-matrix DARC photoionization of the ground and excited states of FeXVII. Photoionisation from every initial level, from the listed configurations and having an overall quantum number between $J = 0$–$4^{o,e}$ is presented. The dense Rydberg structure originates from the 407 final states in the residual ion. The highest n-shell included in the R-matrix calculation has a principal quantum of $n = 5$ and therefore some degree of initial and final state extrapolation is further required for a converged opacity.

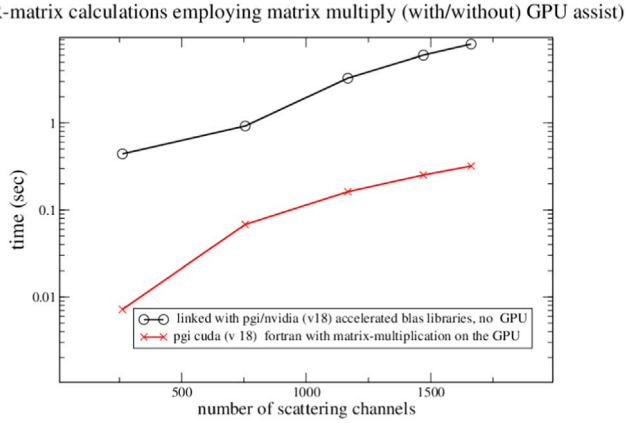

Figure 3. A comparison of the standard parallel R-matrix code versus the parallel R-matrix with GPU implementation as a function of the number of scattering channels. Even for small numbers of scattering channels there is a factor of twenty difference between the two methods. Larger cases will provide better comparisons as the overhead required to move the calculation from the CPU to the GPU will not be as evident in the timings.

factor of between 50 and 100. This has now been implemented within the R-matrix outer region codes that generate photoionization cross sections. The R-matrix itself must be calculated for every photon energy, but can be formulated as a simple matrix multiplication. Figure 3 shows the GPU speed-up obtained for relatively small cases as a function of the number of channels as compared to the DGEMM (matrix-multiply) vendor-supplied accelerated libraries.

4. Solar UV and EUV

Vanessa Polito[1] and Giulio Del Zanna[2]

[1]Bay Area Environmental Research Institute [2]University of Cambridge

Introduction. Since the early 1960s, several spectroscopic and imaging instruments have observed the solar corona from the x-rays to the ultraviolet (XUV). The solar spectrum is in fact rich in UV (900–2000 Å) and extreme ultraviolet (EUV, 150–900 Å) emission lines, which provide important diagnostics of the physical conditions of the plasma in the solar atmosphere. The active (flaring) corona is instead primarily emitting in the soft x-rays (50–150 Å) and x-rays. The validity of these diagnostics crucially depends on the accuracy and completeness of the atomic data used to interpret the spectra so that the technological advancement in instrument development has to be accompanied by a corresponding progress in atomic calculations. For a recent review of past and present observations, spectral diagnostics in the XUV, and progress in atomic data see [36].

In this section, we provide a brief overview of the status of atomic data in the EUV and UV relevant to current and future (planned or proposed) solar spectrometers, and highlight what we think is still needed in order to support the interpretation of the next generation spectroscopic data.

Current and future solar EUV/UV instruments

Hinode EIS and SDO EVE. The Hinode EUV solar spectrometer (EIS, [89] 170–211 Å and 245–292 Å) required a significant amount of work to aid the line identifications and to improve atomic data for the coronal lines. This occurred because of the high-sensitivity, high spectral resolution (60 mÅ) and relatively accurate (stable) radiometric calibration (20%–30%). All the brightest lines have now been identified and line intensities are now well reproduced (within 20% or so) in the EUV, as shown in a recent comparison between quiet Sun medium-resolution (1 Å) SDO/EVE ([37], 1–1050 Å) and simulated spectra using CHIANTI v.10 data [38]. There are still many weaker EUV lines not identified, especially low-temperature ones (see [39]). In a survey of coronal lines, it was shown that about half of the weaker transitions were still unidentified [40]. This problem is partly due to the fact that there are still many ions for which atomic data are not accurate or are missing. The missing identifications and atomic data in the weaker lines has also been highlighted in a series of studies with an EBIT devoted to the identification of spectral lines in the EUV bands of the SDO/AIA [41] imagers, see e.g. [42] and references therein. Atomic data for the soft x-rays were almost completely lacking until recently, with the exception of the high-T flare lines (10–15 MK). A significant improvement for coronal ions was achieved, with new atomic data and new identifications of strong lines (see [40]). However, about a third of the spectral lines still needs identification.

Interface region imaging spectrograph (IRIS). The IRIS ([43]) is a dual spectrograph (SP) and imager (SJI) observing the Sun in two spectral bands: FUV (1332–1358 Å, 1389–1407 Å) and NUV (2783–2834 Å) at unprecedented spatial resolution (0.33″/0.4″), very high spectral resolution (13–26 mÅ) and temporal cadence (down to ∼1–2 s). The main goal of IRIS is to study the interface layer between the chromosphere and the solar corona and thus it mainly observes optically thick emission, which need complex modeling (including radiative transfer) for their interpretation. Nevertheless, several optically thin emission lines are observed by IRIS, including those from Si IV, O IV, S IV, Fe XXI among the strongest. The atomic rates (radiative and collisional) for these ions are generally accurate (20%–30%). However, significant discrepancies (factors of 2–5) between observed and predicted radiances for the some of the low-temperature transition region lines (such as Si IV) are present. This is a known issue which affects measurements of chemical abundances and densities for example. Time-dependent ionization and non-Maxwellian electron distributions are often invoked to explain such discrepancy (see the review by [44]). Density-dependent effects also need to be included in the calculation of the ion CSDs (see a recent example on Carbon [45, 46], on the IRIS lines). In addition, some unidentified (mostly photospheric) lines are present in the 1352–1356 Å spectral region, and become more visible during flares [47]. Finally, a faint hot Mn XVIII ($T \sim 8$ MK) line should be visible at around 1355 Å, and might partially blend Fe XXI redshifted profiles observed above the flare loop tops (e.g. [48]). Atomic data for this line are uncertain.

EUNIS-2. The Extreme Ultraviolet Normal Incidence Spectrograph (EUNIS) is a two-channel imaging spectrograph (89–112 Å and 520–640 Å) currently scheduled for launch on a sounding rocket in 2020. The new 89–112 Å passband will explore this poorly-known spectral region, which has never been observed by an imaging spectrograph before. Interesting lines in this spectral region include flare lines, strong 2-2 transitions in Fe XVIII—Fe XXIII. We expect that the new EUNIS observations will drive further improvements in the atomic data.

Spectral imaging of the coronal environment (SPICE) and the UV. The SPICE ([49]) instrument is one of several remote-sensing instruments built in support of the *in situ* ones aboard Solar Orbiter, the first M-class ESA mission, to be launched in February 2020. Together, the ten Solar Orbiter instruments will provide a complete description of the origin, transport and composition of the solar wind, by reaching a minimum perihelion of 0.28 AU and later raising the orbital plane above the ecliptic. SPICE is an imaging spectrometer in two wavelength bands (704–790 Å and 973–1049 Å) with a spatial resolution at 1 AU of 4″. The spectral bands are well known as they have been observed regularly with previous instruments such as SoHO SUMER. The advantage of SPICE over SUMER will be the possibility to simultaneously observe all the lines at once. The strongest lines are from

simple ions (e.g. Li-like) for which atomic rates ought to be very accurate (10%–20%), but most of the cooler lines are affected by the problems in the CSD we have mentioned. Additionally, significant discrepancies (factors of two) between observed and predicted line intensities in the UV have been reported [50].

Marshall Grazing-Incidence x-ray Spectrometer (MaGIXS). The MaGIXS ([51]) is the first ever x-ray imaging spectrometer designed to observe the solar spectrum in the x-rays, 6–24 Å, at a resolution of about 50 mÅ. The instrument utilizes a novel design, with a set of mirrors producing a stigmatic image of the slit with $\sim 5''$ spatial resolution. MaGIXS is scheduled to fly on a sounding rocket in 2020. The spectral lines emitted in this region cover the 3–15 MK temperature range, and are mostly from Fe XVII to Fe XXIV. The atomic data for these lines are relatively well known as several missions observed this spectral region in the 1970s and 1980s and significant improvements in the Fe XVII and Fe XVIII cross-sections were achieved in the mid-2000 with *R*-matrix scattering calculations (see [36]). Aside from the study of the heating the 3–15 MK plasma, and the possibility to measure relative chemical abundances (e.g. Ne/Fe or O/Fe), MaGIXS should in principle be able to provide some constraints on the presence of non-Maxwellian electrons (see [52]).

Multi-slit solar explorer (MUSE). The MUSE ([53]) is a proposed MIDEX mission, whose design consists of a dual EUV spectrograph and imager with very high spatial ($0.4''$), spectral (14–28 mÅ) and temporal (1–4 s) resolution. MUSE's novel design with 37 slits will provide for the first time simultaneous high resolution spectra over a large field-of-view ($170'' \times 170''$) within 20 s, improving the rastering cadence by almost two orders of magnitude compared to previous EUV spectrometers. MUSE will cover 108 Å (Fe XIX, Fe XXI), 171 Å (Fe IX) and 284 Å (Fe XV) passbands with a FWHM of 2, 4, and 12 Å respectively, providing a range of crucial coronal heating diagnostics.

EUVST. The EUV High-Throughput Spectroscopic Telescope (EUVST) is an M-class mission, which was proposed to the Japanese Space Agency (JAXA) in 2017 and is currently being considered for launch. It consists of a spectrograph and a slit-jaw imaging (SJI) system, observing the Sun at very high spatial resolution ($0.4''$) and cadence (as high as 0.2 s). The spectrograph includes four bands covering a broad spectral range (first order: 170–215, 690–850, 925–1085, 1115–1275 Å; second order: 463–542, 557–637 Å), while the SJI observes the photosphere (2833 Å) and chromosphere (Mg I 2852 Å, Mg II k 2796 Å). EUVST has a strong heritage from Hinode EIS (for the EUV) and SoHO SUMER (for longer wavelengths), covering many strong lines formed over a broad range of temperatures, such as Ne VIII, Fe IX–XIV (0.6–2 MK), Si XII (2 MK) and Fe XVIII–Fe XIX (7–10 MK).

Advances in atomic data. The CHIANTI atomic database and programs (www.chiantidatabase.org) are almost universally used in solar physics for interpreting spectral and imaging data, new missions planning and theoretical modeling (radiative losses and forward modeling). A significant improvement for the coronal lines was achieved with v.8 [54], with data calculated by the UK APAP network (apap-network.org), which has now become the main atomic data provider of cross-sections for the fusion and astrophysics communities. For a review of recent achievements and challenges in such calculations see [55]. For example, it was realized that large-scale *R*-matrix data are required for the 4 to 3 transitions in the soft x-rays; these larger models affected the forbidden UV lines within the lower levels by up to factors of two for some ions. CHIANTI v.9 [56] improved the modeling of the satellite lines, while v.10 will include APAP data for the Mg- and Be-like sequences. Large-scale scattering calculations on the other sequences are needed (some for the simpler ones is on-going). To resolve the line identification problems accurate ab-initio atomic structure data (see [57]) and laboratory measurements (also of rest wavelengths) are needed. Finally, for the well-studied ions, there is a need to assess uncertainties in the atomic rates and how they affect diagnostics, as e.g. in [58].

Concluding remarks. As high-resolution spectroscopy is featuring in all the main upcoming missions, it is clear that significant renewed effort in Laboratory Astrophysics is needed. In particular, to complete the calculations of atomic rates, the identifications of spectral lines, and the assessment of uncertainties in the atomic data. Further efforts are also needed to include more physical processes into the modeling (e.g. density-dependent, out of equilibrium, opacity effects).

Acknowledgments

GDZ acknowledges support from STFC (UK), which has also been funding the UK APAP network. We thank Dr Adrian Daw, Dr Bart De Pontieu and Dr Harry Warren for sharing information about the instruments EUNIS, MUSE and EUVST respectively.

5. X-ray transitions (radiative, collisional)

Liyi Gu[1] and Natalie Hell[2]

[1]RIKEN [2]LLNL

Status. Hot, x-ray emitting plasmas constitute a major component of baryonic matter in the Universe. They are found at all scales, from the Solar system up to the large-scale filaments of the cosmic web. Spectroscopic observations of the x-ray transitions from these plasmas hold keys to advance our understanding of their nature. A good example is on the study of the AGNs, which are accreting supermassive black holes at the centers of galaxies. Thanks to the high-resolution spectrometers onboard Chandra, XMM-Newton, and Hitomi satellites, it has been discovered that the AGNs are pumping out a mixture of cold/hot plasma and jets, which remove a substantial amount of cooling gas in the environment, affecting the evolution of the host galaxies and galaxy clusters on cosmological timescales; meanwhile, such AGN 'feedback' processes must be dynamically gentle, as the environmental turbulence is found to be low [59]. Fundamental to these exciting discoveries are spectral signatures from a set of x-ray emission and absorption lines from the AGNs and their surroundings.

Recently, the sensitivity and resolution of x-ray spectrometers have increased so much that our ability to explore the Universe further is limited by the accuracy of the atomic modeling of the x-ray transitions. The Hitomi results on the Perseus cluster showed surprising differences between the predictions by the best plasma codes, for instance 15% for the derived iron abundance, while its statistical uncertainty from the instrument is only 1% [60]. These differences depend on only a small number of x-ray transitions, mostly the electron-impact excitation cross sections and the radiative decay rates.

Current and future challenges. The XRISM is a successor of Hitomi and is expected to launch in 2022. It will provide non-dispersive high-resolution x-ray spectra over the 0.3–20 keV band, with spectra of unsurpassed quality, particularly in the Fe-K band near 6 keV. Optimizing the XRISM science outcome will require that analysis tools, centered on the plasma codes of x-ray transitions, be capable of reliably modeling and interpreting the XRISM data. Several specific requirements for atomic data are listed below.

The accuracy of transition energies directly determines our ability to trace plasma motion through Doppler-shift. XRISM science requires the transition energies to be known to an accuracy of 10^{-5}–10^{-3}, depending on the specific science cases. The line energies of highly ionized species (H-like and He-like) are already accurately determined, both theoretically and experimentally, with uncertainties $\leqslant 10^{-4}$. The main challenges are the species with mid-to-low ionization states. For instance, the transition energies of the Fe II fluorescent Kα lines are known theoretically to a level of 10^{-3}–10^{-2} [61]. The calculations of the inner-shell Fe-L transitions are accurate to a similar level, with only a limited number of experimental benchmarks.

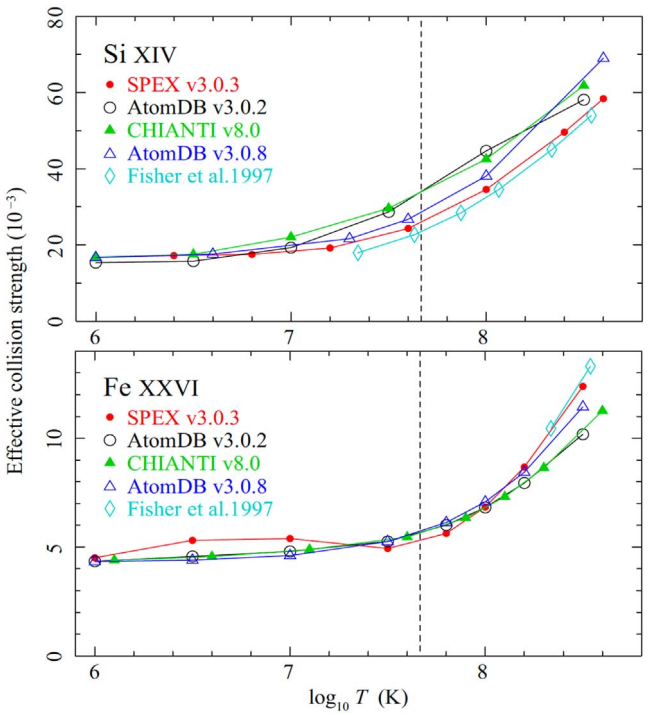

Figure 4. Comparisons of effective collision strength as a function of balance temperature, for the combined Lyα1 and Lyα2 transitions [60]. The vertical dashed line marks 4 keV. Reproduced from [60]. CC BY 4.0.

The electron-impact excitation and radiative decay rates are often the dominant processes for line emission from collisional plasma. To ensure the XRISM results on, e.g. the elemental abundances of galaxy clusters are not limited by atomic uncertainty, the excitation cross section and radiative transition probabilities are required to be accurate at a ~10% level. This is currently challenging, because the comparison of different calculations on the H- and He-like Si, S, Ar, Ca, and Fe effective excitation strength shows uncertainties on the level of 20%–40% ([60], figure 4), and the Ne-like Fe excitation rates are known theoretically to ~20% [62]. The oscillator strength ratio of the leading Ne-like Fe lines measured using x-ray laser spectroscopy was found to be 3.6σ lower than the theoretical value [22].

The XRISM mission, but also the later Athena mission (launch 2030), have recognized the crucial role of accurate atomic data for x-ray transitions. Note that Athena has a spectral resolution three times better than XRISM, requiring more stringent atomic accuracy by nearly the same factor.

Advances in science and technology to meet challenges. The path to accurate atomic data that fulfils the identified data needs is twofold: fully utilizing existing capabilities that are already up to the task; and developing new capabilities where desired accuracies cannot yet be met. Laboratory measurements as well as atomic physics theory and calculations are both integral parts of fulfilling these needs. For atomic databases to be as complete as possible, they have to rely heavily on accurate theoretical calculations. Experiment and theory only together further our

understanding of atomic physics. Some measurements rely on theory, e.g. for line identification or as part of the analysis. Conversely, in the absence of experimental benchmarks, it is challenging to assess the accuracy of the calculations.

On the experiment side, tokamaks and EBITs are closest to the temperature and density parameter space covered by astrophysical plasmas [17], and are versatile tools that cover a wide range of atomic physics parameters relevant for collisional astrophysical plasmas. While tokamaks produce thermal plasmas, an EBIT emits x-rays following the interaction of trapped ions with a quasi-monoenergetic electron beam that allows to probe atomic physics parameters as a function of electron energy for a chosen narrow range of ion species. Measurements at either x-ray source rely heavily on state-of-the art x-ray spectrometers. In order to maintain the ability to follow up on new spectral features discovered by x-ray observatories in space, it is therefore important that the spectrometers employed in the lab advance with and at least match the capabilities of space instrumentation, especially in terms of spectral resolution. However, the extremely high resolution of proposed grating spectrometers such as on Arcus and Lynx will rival that of the current highest-resolution spectrometers in the laboratory.

Transition energies can be measured on many laboratory x-ray sources. They are usually calibrated relative to well-known reference lines, mostly in the He- and H-like Rydberg series, i.e., they are ultimately limited by the accuracy of the calibration lines. More concerning, however, is that measurements for lower charge states are largely missing—a problem solvable with current facilities, but requiring an increase in resources allocated, such as time and manpower—and that resolving heavy line blends such as, e.g. K-shell transitions of near-neutral ions, is taxing even for the highest available resolving powers.

Using resonant photoexcitation by coupling an EBIT to a brilliant x-ray light source can achieve 70 meV accuracies for transition energies [22, 63] and directly probes natural line widths and oscillator strength ratios [63].

Measurements of collisional excitation cross sections are more difficult to incorporate directly into plasma models, but are important benchmarks and can be used to tweak the theory values. Absolute excitation cross sections for EUV and x-ray transitions in highly charged ions have only been measured with EBITs [64]. Crossed- or merged-beam measurements are only available for neutrals up to a few hundred eV electron impact energies or for $\Delta n = 0$ transitions in the optical/UV up to a few 10 eV electron energy [64, 65]. Cross sections using EBITs are measured to $\sim$10% and can be done for electron energies ranging from about 100 eV to over 100 keV, but so far only exist for a few ions and electron impact energies [64]. The largest contribution ($\sim$5%) to their uncertainty is due to the correction for the polarization of radiation emitted by an EBIT. Excitation cross section measurements would thus benefit from improving polarization measurements and calculations to better than 20%. Again, measurements for inner-shell transitions and intermediate charge states are largely missing. These are challenging due to a strong excitation component from inner-shell ionization, whose relative contribution depends on the charge balance. Disentangling the cross sections for these two channels requires a modified, more complex approach.

Future observations will be sensitive to spectral signatures of deviations from thermal energy distributions. EBITs ability for fast 'sweeps' of the electron energy facilitates an effective simulation of a variety of energy distributions in the lab [66], suitable to study their effects on line ratios and to test corresponding plasma models. Including energy-dependent cross sections in the databases would aid in accommodating such plasma models.

On the theory side, several well established codes exist. For example, MBPT and MRMP codes achieve accuracies for transition energies on the 10^{-4} level. However, measurements suggest that the uncertainties [22] of the calculated oscillator strengths, especially for transitions with strong level mixing, are dominated by inaccuracies in the wavefunctions themselves when including mixing only among a limited number of levels. Excitation cross section calculations can disagree by 20% or more; however, *R*-matrix codes are estimated to achieve 10% accuracies if a sufficient number of levels is included to allow proper convergence [67]. Speed and complexity of the codes benefit from continued adaptation to advances in computer architecture. Most theoretical studies concentrate on H-, He-, and Ne-like ions. While some calculations for open-shell ions and inner-shell transitions have become available more recently, their selection is much more limited.

As described, many capabilities already exist to provide the needed atomic data and are waiting to be used; other areas would benefit from further advances to push the limits of achievable accuracy. All have in common that they require fundamental long-term support, including for maintenance and upgrades, beyond funding for individual projects. This is true for experiments as well as theory, databases, and models. Sufficient support for a larger work force, including training students, would help complete the task in time for XRISM.

Concluding remarks. By introducing significant systematic uncertainties to the spectral analysis [60], the current state of our atomic reference data limits the conclusions we can draw from observations with next-generation high-resolution x-ray observatories such as XRISM and Athena. A concerted effort to improve the atomic data and plasma models—in close collaboration between experimentalists, theorists, and observers, both in preparation to and after launch—is paramount to ensure we can take full advantage of the capabilities of these new observatories.

Acknowledgments

Liyi Gu acknowledges the RIKEN Special Postdoctoral Researcher Program. Work at LLNL was performed under the auspices of the US DOE under Contract No. DE-AC52-07NA27344.

6. Charge exchange

Renata Cumbee[1] *and Gabriele Betancourt-Martinez*[2]

[1]NASA/GSFC [2]IRAP/CNRS

Status. Charge exchange (CX), or charge transfer, is the radiationless transfer of one or more electrons from a neutral atom or molecule to a highly charged ion during a close interaction. The electron is typically captured into a highly excited state and subsequently radiatively de-excites, producing characteristic line emission observable in the x-ray and EUV bands. These lines can be diagnostic of the neutral species, the ion charge state, their densities, and their collision velocity. Though CX has been studied by plasma physicists for decades, it was not until the 1996 discovery of cometary x-rays due to charge exchange with solar wind ions that the process became of wider interest to the x-ray astrophysics community. Now it is well known that CX occurs frequently throughout the solar system and also contributes a temporally variable x-ray foreground to all observations [68]. It may also occur astrophysically, for example in supernova remnants, galactic and stellar winds, and galaxy clusters. Since CX is a recombination process, the resulting spectra are very distinct from those resulting from collisional excitation (see figure 5). With upcoming missions such as XRISM and Athena, which will be equipped with non-dispersive, high-resolution spectrometers, it is very likely that we will be routinely measuring CX at some level, whether in the foreground or as part of the observation target. It is thus imperative to have a complete and accurate understanding of the spectral signatures of CX and how to properly interpret its diagnostics.

Total CX cross sections, important for predicting the absolute strength of the CX contribution in an observation, have been known fairly accurately for decades, but quantum state-resolved cross sections, which are needed for accurate spectral modeling, remain elusive. These n, ℓ, and S or j-resolved cross sections are the first step in producing theoretical CX x-ray emission spectra. The x-ray spectrum is then created by performing a radiative cascade from the initial excited state. There are various approaches for producing these state-resolved cross-sections, but no single method is appropriate for the wide range of energies relevant for astrophysics. The largest database of $n\ell$S-resolved charge exchange cross sections to date, Kronos [69], is primarily based on the Multi-Channel Landau–Zener (MCLZ) theory. This theoretical method produces n-resolved cross-sections for CX with bare ions (explicit ℓ-resolved calculations are not calculated for bare ions due to the degeneracies in ℓ-levels for a given n-level for H-like ions.), and then an appropriate ℓ-distribution is applied, as described by Mullen *et al* 2017 [69] and Smith *et al* 2014 [70].

When the initial ion is not bare, MCLZ theory produces explicit n,ℓ, and S resolved cross-sections. While this method relies on some approximations, the resulting spectra often agree with laboratory benchmarks [69]. The MCLZ approach has been streamlined and is readily available for calculating

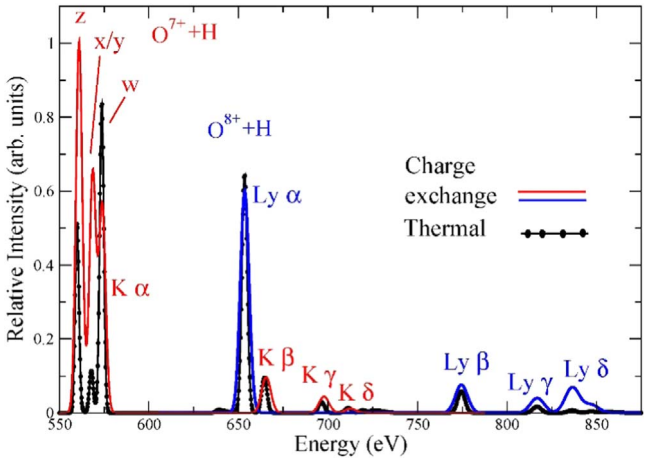

Figure 5. Simulated spectra resulting from CX and thermal emission for the same ions. For K-shell ions undergoing CX at low collision velocities, the typical spectral diagnostics for CX include an enhanced 'forbidden' (z) line in the He-like K-alpha triplet and a strong high-n Lyman line (here, Ly-δ).

cross-sections for many ions (H-like and He-like C-Si, Fe), neutral targets (H, He, H_20, CO_2, CO) and at a large range of collision velocities relevant to astrophysics. Where possible, the MCLZ calculations in the Kronos database are supplemented by more rigorous methods, including the Quantum-mechanical Molecular Orbital Close-Coupling (QMOCC) method, accurate from the lowest energies to ~1 keV/u, the Atomic-Orbital Close-Coupling (AOCC) method, accurate from intermediate/high energies (~100 eV/u to ~500 keV/u), as well as the classical trajectory Monte-Carlo method, appropriate for higher energies (~5 keV/u to ~10 MeV/u). In order to verify the reliability of these data, it is imperative that we continue to benchmark these data to experiments as often as possible.

Recent advancements in astrophysical spectral synthesis codes have made it easier for astronomers to use CX models when comparing to astrophysical data. Both the SPEX-CX [71] model and the AtomDB CX V2 (ACX2) [70] model use theoretical CX cross-sections to model CX for many important ions. The SPEX-CX model uses theoretical cross-sections collected from the literature, and the ACX2 package uses MCLZ data from the Kronos database for H-like and He-like ions. For ions without specific cross sections, both codes apply empirical formulae to calculate the distribution of the n and l capture states. SPEX further applies scaling relations in certain cases.

There are various ways to experimentally study CX. For example, one can use an EBIT to stimulate CX collisions at low velocities (a few 10 s eV/u) [72]. One can also generate an ion beam by EBIT ion extraction or with electron cyclotron resonance sources. These ion beams can be guided towards a source of neutrals—either a neutral gas cell or a neutral beam—in order to perform CX experiments at varying collision velocities of a few 100–10 000s eV/u [73]. These methods, combined with a spectrometer, provide us with photon emission spectroscopy. In some cases, it is possible to deduce total or state-selective capture cross sections directly

from the spectra, but this often depends on our knowledge of branching ratios. Especially versatile, COLTRIMS experiments [74] utilize a merged-beam apparatus combined with analysis of the final projectile and target charge states and time-of-flight measurements. This combination of tools provides us with CX spectra, relative *n*-resolved cross sections, and the relative contribution of single versus multiple electron capture (SEC, MEC).

Current and future challenges. While a robust database of CX cross-sections for H- and He-like ions with various neutral targets exists, the data are far from complete. For example, the majority of theoretical cross sections are calculated assuming SEC, when it has been shown experimentally that MEC can be just as important [74]. Similarly, there are very few data from experiments that can distinguish between the two processes. In addition, most theoretical approaches are optimized for low-Z ions in LS coupling, and can not be immediately translated to jj coupling, appropriate for mid- to high-Z ions.

Experimental benchmarks to models are critical for determining their strengths and limitations, but more are needed. Low velocity CX spectra, such as those measured from EBIT experiments, have proved especially difficult to model with available theoretical approaches. Applying the most easily available ACX and SPEX CX models that use simple scaling relations often can not reproduce these data [75]; see figure 6. These experiments have also shown that for CX capture onto bare ions, the relative strength of the high-*n* emission varies more than models predict, and does not scale with parameters such as the atomic number of the ion, or the ionization potential of the neutral [76]. Often, only the most computationally expensive methods such as QMOCC and AOCC reproduce experimental spectra or trends in line ratios [73], but these theoretical data are quite sparse.

One of the biggest current challenges is collecting experimental data with atomic H. This is the most astrophysically relevant neutral partner, and also the only way to ensure primarily SEC. However, it is extremely difficult to produce atomic H gas for a CX experiment in sufficient quantities; virtually no data exist in the literature. We thus have no means of benchmarking the most well-understood theoretical calculations.

Advances in science and technology to meet challenges. In order to be able to identify and fully understand the CX contribution in current and future x-ray observations, as well as better understand its diagnostic potential, our knowledge of the atomic processes involved in CX must improve. Advancements in computational methods are required to make QMOCC and AOCC calculations more readily available. Various theoretical approaches need to be adapted for handling MEC, and similarly, improved computational methods are necessarily to include the large number of energy levels involved during electron capture. Modeling CX for highly charged ions is difficult in part because of the large number of available capture states. Further, electron

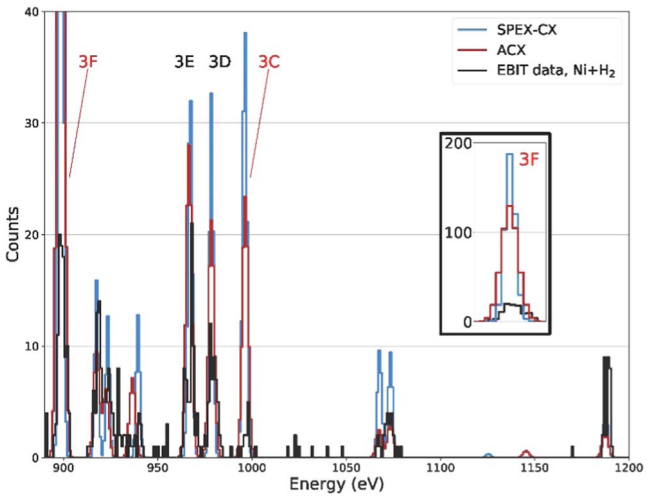

Figure 6. EBIT CX data (black) of Ne-like Ni undergoing CX with neutral H_2 is not well reproduced by ACX and SPEX-CX models (colors). Reproduced from [75].

configuration mixing between capture states of differing energy levels is likely important [75] but many current theoretical methods have to limit the number of states allowed to mix to decrease computational time. Other theoretical advancements required for CX include more accurate energy level calculations for He-like and lower charge states, especially for high-Z ions that will become more relevant with XRISM and Athena observations.

For the most part, experimental methods required to benchmark models exist, but increased funding is needed to be able to perform them. Ideally, CX experiments would be performed for many ions colliding with neutral H at various collision velocities, as well as experiments disentangling MEC from SEC. This requires the use of a merged beam line to vary collision velocities, combined with a COLTRIMS setup to measure the ion/neutral post-collision charge state. A calorimeter detector provides high resolution and a wide bandpass for resolving high-*n* to ground transitions. With this combination of tools, we can measure state-selective cross sections as a function of velocity and ion. The drawback with this experiment is that emission from metastable states, like the He-like forbidden line, is not detected with the standard setup. While modifications to this standard setup are investigated, these experiments can be supplemented with EBIT measurements to determine the ratio between the K-alpha lines at low collision velocities.

Concluding remarks. The diagnostic power of CX in our current and future observations can only be fully harnessed once we have a better understanding of the underlying atomic physics. We also risk misinterpreting important physical parameters by applying inaccurate models to our spectra. Increased programmatic support is crucial to be able to perform the necessary experiments and modeling to be ready for future missions.

Acknowledgments

The authors gratefully acknowledge M Leutenegger for helpful discussions. RC is supported by an appointment to the NASA Postdoctoral Program at NASA/GSFC, administered by the Universities Space Research Association and with a Chandra Grant.

7. X-ray extinction by interstellar dust: experimental studies and future facilities

Elisa Costantini[1] *and Lia Corrales*[2]

[1]SRON Netherlands Institute for Space Research [2]University of Michigan

Evidence of extinction by interstellar dust in the x-ray band. Early x-ray observations pointed out the influence of the interstellar medium on the x-ray spectra of background sources. The intervening gas and dust imprints deep edge-like features on the spectrum, due to the photoelectric effect caused by the interaction between the x-ray and the electrons in the gas atoms. The energy at which interstellar absorption features appear reflects the chemical composition of the medium. The x-ray band covers the energy of the K- or L-shell transitions of the most abundant interstellar metals: C, N, O, Fe, Ne, Si and Mg. The absorption features bear a powerful diagnostic on the characteristics of the intervening medium: abundances, depletion (fraction of a certain element included in dust particles), chemical composition and even crystallinity and size distribution of dust can be in principle inferred using high-resolution x-ray spectroscopy (e.g. [18, 77]).

Photoelectric features can be significantly modified when absorption is caused by solid dust grains rather than gas. When an incoming x-ray photon interacts with an electron inside the grain, the resulting photo-electron wave interacts with the neighboring waves, creating an interference pattern. Such pattern is dependent on the lattice configuration, i.e. the chemistry of the grain (figure 7). The complex refractive index of the material $m = n + ik$, where n and k are the optical constants, describes the two elements of dust extinction: scattering and absorption. The scattering feature of a material, which mimics the appearance of an emission peak at the energy of the edge, is a diagnostic of the dust size distribution of the bulk material interacting with the x-rays (e.g. [78]).

Depletion measurements indicate that solid phase materials in the interstellar mediums are mainly comprised of carbon (e.g. graphite, amorphous/hydrogenated carbon, nano-diamonds) and the group O, Fe, Mg and Si, which form the silicates (sometimes with Ca and Al inclusions). Oxides, e.g. O bound with Fe, S, Si, Mg etc, and sulfates (e.g. FeS) may also be present (e.g. [79]).

The brightest local point sources—x-ray binaries, where a neutron star or black hole is accreting from a companion star—provide the most promising datasets for studying ISM absorption features. Currently, the highest resolution x-ray spectra available are obtained with gratings instruments equipped on the Chandra x-ray Observatory (5–15 mÅ resolution in HETG, 50 mÅ resolution in LETG) and XMM-Newton RGS (10–50 mÅ resolution). Over the past 20 years, they have enabled breakthrough study in solid phase signatures of astrophysical dust (e.g. [80]). However, many early works provided only an empirical model for the location of dust features, and it has been suggested that some features

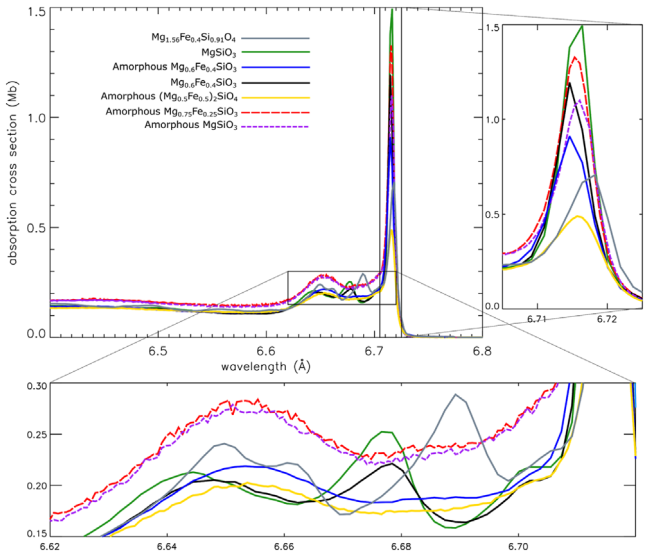

Figure 7. Fluorescent spectrum of a set of silicate samples for the Si K-edge at 1.84 keV = 6.74 Å (adapted from [17]).

attributed to dust are instead low-ion states of the gas phase ISM (e.g. [81]). Strong conclusions about the mineralogy of astrophysical dust cannot be made without high resolution measurements of the cross-sections for astrophysically relevant materials.

Advances in laboratory measurements of interstellar dust analogs. A large campaign of laboratory measurements of interstellar dust analogs has been recently carried out in order to create a meaningful data base of interstellar dust extinction profiles to interpret the astronomical data. Other specific measurements are described in [77, 82, 83].

Twenty samples of silicates (olivines and pyroxenes) with different Mg:Fe ratios and varying crystallinity have been measured in the laboratory, together with oxides [17]. Carbonaceous materials—graphite, amorphous carbon, and SiC—are being prepared for upcoming measurements.

Depending on the energy of the photoelectric transition, different facilities may be used to characterize the dust sample.

High energy features in the x-ray band (e.g. Fe K-edge at 7.1 keV) have been characterized using the Dubble beamline at the European Synchrotron Radiation Facility in Grenoble, France, which provides an energy resolution of 0.3 eV. A fine-grained sample is pressed into a pellet and scanned by the x-ray beam, creating in output a transmission spectrum [84].

X-ray transitions in the 1–4 keV range can be best observed using facilities like the LUCIA beam line at the Soleil synchrotron in Paris, France. In this case a fluorescence experiment is used. The x-rays in the beam interact with the fine-grained sample, which has been pressed into an indium foil, producing a fluorescence spectrum. The energy resolution provided by this beamline is 0.25 keV.

Low energy features (C, O K-edge and Fe L-edges) are best characterized using lower energy sources. In this case the TITAN scanning transmission electron microscope at the University of Cadiz, Spain, is being used. The measurements

are performed through the electron energy loss spectroscopy technique, one grain at a time. The resulting spectrum is derived considering the change in velocity of the electrons caused by inelastic scattering within the material. The energy resolution is about 0.25 eV.

Calculating optical constants from the high resolution laboratory data is also necessary for fully modeling the effects of x-ray attenuation—the combination of absorption and scattering—which depends on both telescope imaging resolution and the location of the dust [78]. These optical constants are also necessary for measuring attenuation features that arise from non-spherical dust grains [85] or to distinguish among the mixed-composition dust grain models that have been constructed to from longer wavelength observations.

Future prospects for observing interstellar dust. When designing x-ray observatories of broad interest to the high energy astrophysics community, two leading methods of high resolution x-ray spectroscopy dominate. Each of these present tradeoffs for the study of solid phase materials in space. An array of x-ray microcalorimeters, equipped on *Hitomi* , the x-ray Imaging Spectroscopy Mission (XRISM, launching 2022), and *Athena* (launching 2028), provide 1–5 eV spectroscopic resolution from each pixel in the image, a factor of 30, over most of the x-ray band, better than the CCD instruments currently in use. Unlike gratings observations, microcalorimeters could be used to measure dust signatures in x-ray scattering halos that arise from individual foreground clouds (e.g. [86]), and offer one of the few ways to probe large micron-sized grains in the ISM. However, many of the microcalorimeter missions have small effective areas at the C K and O K photoabsorption regions. More importantly, with fixed energy resolution, microcalorimeters provide poorer resolution spectra of C and O, the two most abundant interstellar elements, in comparison to gratings instruments.

New critical-angle transmission gratings can provide 2 mÅ resolution or better [87] at the energies associated with C, O, and Mg K shell, and Fe L shell photoabsorption. Concept missions such as ARCUS and *Lynx* would use these gratings to measure dust XAFS in fine detail. In addition to measuring the solid-phase composition of the two most abundant interstellar metals, C and O, high throughput x-ray gratings missions provide the potential to measure the mineralogical composition of dust in quasar absorption line systems.

Conclusions. The x-ray band offers a unique test bed for probing the chemical and physical characteristics of interstellar dust.

Upcoming x-ray missions will provide unprecedented sensitivity and energy resolution that have to be matched with adequate theoretical calculations and laboratory measurements.

Acknowledgments

EC is partially supported by the NWO-VIDI grant 639.042.525.

ORCID iDs

Randall Smith https://orcid.org/0000-0003-4284-4167
Natalie Hell https://orcid.org/0000-0003-3057-1536

References

[1] Muller A 2008 Electron-ion collisions: fundamental processes in the focus of applied research *Adv. At. Mol. Opt. Phys.* **55** 293–416
[2] Dere K P 2007 Ionization rate coefficients for the elements hydrogen through zinc *Astron. Astrophys.* **466** 771–92
[3] Urdampilleta I, Kaastra J S and Mehdipour M 2017 X-ray emission from thin plasmas. Collisional ionization for atoms and ions of H to Zn *Astron. Astrophys.* **601** 85
[4] Loch S, Pindzola M, Ballance C, Witthoeft M, Foster A, Smith R and O'Mullane M 2013 The propagation of uncertainties in atomic data through collisional-radiative models *AIP Conf. Proc.* **1545** 242–51
[5] Hahn M 2014 Electron impact ionization of stored highly charged ions *J. Phys.: Conf. Ser.* **488** 012050
[6] Garcia-Rojas J, Pena M, Morisset C, Delgado-Inglada G, Mesa-Delgado A and Ruiz M T 2013 Analysis of chemical abundances in planetary nebulae with [WC] central stars: II. Chemical abundances and the abundance discrepancy factor *Astron. Astrophys.* **558** 122
[7] Badnell N R, O'Mullane M G, Summers H P, Altun Z, Bautista M A, Colgan J, Gorczyca T W, Mitnik D M, Pindzola M S and Zatsarinny O 2003 Dielectronic recombination data for dynamic finite-density plasmas *Astron. Astrophys.* **406** 1151–65
[8] Schippers S 2015 Electron-ion merged-beam experiments at heavy-ion storage rings *Nucl. Instrum. Methods* B **350** 61–5
[9] Vernazza J E and Raymond J C 1979 On the ionization equilibrium balance *Astrophys. J.* **228** L89
[10] Korol A V, Gribakin G F and Currell F J 2006 Effect of target polarization in electron-ion recombination *Phys. Rev. Lett.* **97** 223201
[11] Hahn M, Muller A and Savin D W 2017 Electron-impact multiple ionization cross sections for atoms and ions of helium through zinc *Astrophys. J.* **850** 122
[12] Hahn M and Savin D W 2015 A simple method for modeling collision processes in plasmas with a kappa energy distribution *Astrophys. J.* **809** 178
[13] Morrison R and McCammon D 1983 *ApJ* **270** 119–22
[14] Schattenburg M L and Canizares C R 1986 *ApJ* **301** 759
[15] Wilms J, Allen A and McCray R 2000 *ApJ* **542** 914–24
[16] Gatuzz E and Churazov E 2017 *The X-ray Universe* p 87
[17] Zeegers S T, Costantini E, de Vries C P, Tielens A G G M, Chihara H, de Groot F, Mutschke H, Waters L B F M and Zeidler S 2017 *Astron. Astrophys.* **599** A117
[18] Beiersdorfer P 2003 *ARAA* **41** 343
[19] Kallman T R and Palmeri P 2007 *Rev. Mod. Phys.* **79** 79
[20] Foster A R *et al* 2011 *2010 NASA Laboratory Astrophysics Workshop* C2
[21] Schippers S *et al* 2016 *Contemp. Phys.* **57** 215
[22] Bernitt S *et al* 2012 *Nature* **492** 225
[23] Müller A *et al* 2017 *ApJ* **836** 166
[24] Bizau J M *et al* 2015 *Phys. Rev.* A **92** 23401
[25] Starace A F 1982 *Theory of Atomic Photoionization, Handbuch der Physik* vol 31 ed W Mehlhorn (Berlin: Springer) pp 1–121
[26] Gu M F 2008 *Can. J. Phys.* **86** 675–89
[27] Badnell N R 2008 *Comput. Phys. Commun.* **182** 1528–35
[28] Kheifets A S and Bray I 1998 *Phys. Rev.* A **58** 4501
[29] Pindzola M S *et al* 2007 *J. Phys. B: At. Mol. Opt. Phys.* **40** R39
[30] Ballance C P and Griffin D C 2006 *J. Phys. B: At. Mol. Opt. Phys.* **39** 3617
[31] http://connorb.freeshell.org
[32] McLaughlin B M, Stancil P C, Sadeghpour H R and Forrey R C 2017 *J. Phys. B: At. Mol. Opt. Phys.* **50** 114001
[33] McLaughlin B M and BBallance C P 2012 *J. Phys. B: At. Mol. Opt. Phys.* **45** 085701
[34] Ballance C P and McLaughlin B M 2015 *J. Phys. B: At. Mol. Opt. Phys.* **48** 085201
[35] Berrington K A, Eissner W B and Norrington P H 1995 *Comput. Phys. Commun.* **92** 290–420
[36] Del Zanna G and Mason H E 2018 Solar UV and x-ray spectral diagnostics *LRSP* **15** 5D
[37] Woods T N *et al* 2012 Extreme ultraviolet variability experiment *(EVE) on the* solar dynamics observatory *(SDO):* overview of science objectives, instrument design, data products, and model developments *Sol. Phys.* **275** 1–2
[38] Del Zanna G 2019 The EUV spectrum of the Sun: quiet- and active-Sun irradiances and chemical composition *A&A* **624A** 36D
[39] Landi E and Young P R 2009 *ApJ* **706** 1
[40] Del Zanna G 2012 Benchmarking atomic data for the CHIANTI atomic database: coronal lines observed by Hinode EIS *A&A* **537A** 38D
[41] Lemen J R *et al* 2012 The atmospheric imaging assembly (AIA) on the solar dynamics observatory (SDO) *Sol. Phys.* **275** 17
[42] Träbert E, Beiersdorfer P, Brickhouse N S and Golub L 2014 High-resolution laboratory spectra of the λ193 channel of the atmospheric imaging assembly instrument on board solar dynamics observatory *ApJSS* **215** 6
[43] De Pontieu B *et al* 2014 The interface region imaging spectrograph (IRIS) *Sol. Phys.* **289** 7
[44] Dudık J *et al* 2017 Nonequilibrium processes in the solar corona, transition region, flares, and solar wind (Invited review) *Sol. Phys.* **292** 100
[45] Dufresne R P and Del Zanna G 2019 Modelling ion populations in astrophysical plasmas: carbon in the solar transition region *A&A* (accepted) (https://doi.org/10.1051/0004-6361/201935133)
[46] Polito V *et al* 2016a Density diagnostics derived from the O IV and S IV intercombination lines observed by IRIS *A&A* **594A** 64P
[47] Polito V *et al* 2016b Simultaneous IRIS and hinode/EIS observations and modelling of the 2014 October 27 X2.0 class flare *ApJ* **816** 89P
[48] Polito V *et al* 2018 Possible signatures of a termination shock in the 2014 March 29 X-class flare *ApJ* **865** 161
[49] Anderson M *et al* 2019 The Solar Orbiter SPICE instrument—an extreme UV imaging spectrometer (https://doi.org/10.1051/0004-6361/201935574)
[50] Doschek E E, Laming J M, Doschek G A, Feldman U and Wilhelm K 1999 *ApJ* **518** 909
[51] Kobayashi K *et al* 2018 The marshall grazing incidence x-ray spectrometer (MaGIXS) *Proc. SPIE* **10699** 1069927
[52] Dudík J *et al* 2019 Signatures of the κ non-Maxwellian in optically thin line spectra: II. Synthetic Fe XVII–XVIII x-ray coronal spectra and predictions for the Marshall Grazing-Incidence x-ray Spectrometer (MaGIXS) *A&A* **626** 88
[53] De Pontieu B *et al* 2019 The multi-slit approach to coronal spectroscopy with the multi-slit solar explorer (MUSE) arXiv:1909.08818
[54] Del Zanna G *et al* 2015 CHIANTI—an atomic database for emission lines. Version 8 *A&A* **582A** 56D
[55] Badnell N R *et al* 2016 Atomic processes for astrophysical plasmas *J. Phys. B: At. Mol. Opt. Phys.* **49** 094001
[56] Dere K P *et al* 2019 CHIANTI—an atomic database for emission lines. XV. Version 9, improvements for the x-ray satellite lines *ApJS* **241** 22D

[57] Jonsson P *et al* 2017 Multiconfiguration dirac-hartree-fock calculations with spectroscopic accuracy: applications to astrophysics *Atoms* **5** 1

[58] Yu X *et al* 2018 Incorporating uncertainties in atomic data into the analysis of solar and stellar observations: a case study in Fe XIII *ApJ* **866** 14

[59] Hitomi collaboration 2016 The quiescent intracluster medium in the core of the Perseus cluster *Nature* **535** 117

[60] Hitomi collaboration 2018 Atomic data and spectral modeling constraints from high-resolution x-ray observations of the Perseus cluster with Hitomi *Publ. Astron. Soc. Japan* **70** 12

[61] Palmeri P *et al* 2003 Modeling of iron K lines: radiative and Auger decay data for Fe II-Fe IX *Astron. Astrophys.* **410** 359

[62] Gu L *et al* 2019 X-ray spectra of the Fe-L complex *Astron. Astrophys.* (accepted) (https://doi.org/10.1051/0004-6361/201833860)

[63] Rudolph J *et al* 2013 X-ray resonant photoexcitation: linewidths and energies of Kα transitions in highly charged Fe ions *Phys. Rev. Lett.* **111** 103002

[64] Chen H and Beiersdorfer P 2008 Electron-impact excitation cross-section measurements at EBITs from 1986 to 2006 *Can. J. Phys.* **86** 55

[65] Phaneuf R A, Havener C C, Dunn G H and Müller A 1999 Merged-beam experiments in atomic and molecular physics *Rep. Prog. Phys.* **62** 1143

[66] Savin D W *et al* 2000 Simulating a Maxwellian plasma using an electron beam ion trap *Rev. Sci. Instrum.* **71** 3362

[67] Smith R K and Brickhouse N S 2014 Atomic data needs for understanding x-ray astrophysical plasmas *Adv. At. Mol. Opt. Phys.* **63** 271

[68] Snowden S L, Collier M R and Kuntz K D 2004 XMM-Newton observation of solar wind charge exchange emission *Astrophys. J.* **610** 1182

[69] Mullen P D, Cumbee R S, Lyons D, Gu L, Kaastra J, Shelton R L and Stancil P C 2017 Line ratios for solar wind charge exchange with comets *Astrophys. J.* **844** 7

[70] Smith R K, Foster A R, Edgar R J and Brickhouse N S 2014 Resolving the origin of the diffuse soft x-ray background *Astrophys. J.* **787** 77

[71] Gu L, Kaastra J and Raassen A J J 2016 Plasma code for astrophysical charge exchange emission at x-ray wavelengths *Astron. Astrophys.* **588** A52

[72] Wargelin B J, Beiersdorfer P and Brown G V 2008 EBIT charge-exchange measurements and astrophysical applications *Can. J. Phys.* **86** 151–69

[73] Defay X, Morgan K, McCammon D, Wulf D, Andrianarijaona V M, Fogle M, Seely D G, Draganić I N and Havener C C 2013 X-ray emission measurements following charge exchange between C 6+ and He *Phys. Rev.* A **88** 052702

[74] Ali R, Beiersdorfer P, Harris C L and Neill P A 2016 Charge-exchange x-ray spectra: evidence for significant contributions from radiative decays of doubly excited states *Phys. Rev.* A **93** 012711

[75] Betancourt-Martinez G L, Beiersdorfer P, Brown G V, Cumbee R S, Hell N, Kelley R L, Kilbourne C A, Leutenegger M A, Lockard T E and Porter F S 2018 High-resolution charge exchange spectra show striking differences from models *Astrophys. J. Lett.* **868** L17

[76] Betancourt-Martinez G L, Beiersdorfer P, Brown G V, Kelley R L, Kilbourne C A, Koutroumpa D, Leutenegger M A and Porter F S 2014 Observation of highly disparate K-shell x-ray spectra produced by charge exchange with bare mid-Z ions *Phys. Rev.* A **90** 052723

[77] Lee J C *et al* 2009 Condensed matter astrophysics: a prescription for determining the species-specific composition and quantity of interstellar dust using x-rays *Astrophys. J.* **702** 970–9

[78] Corrales L R *et al* 2016 The dust-scattering component of x-ray extinction: effects on continuum fitting and high-resolution absorption edge structure *Mon. Not. R. Astron. Soc.* **458** 1345–51

[79] Tielens A G G M, Waters L B F M and Bernatowicz T J 2005 Origin and evolution of dust in circumstellar and interstellar environments *Chondrites and the Protoplanetary Disk* (*Astronomical Society of the Pacific Conference Series* vol 341) ed A N Krot *et al* p 605

[80] Costantini E *et al* 2012 XMM-Newton observation of 4U 1820-30. Broad band spectrum and the contribution of the cold interstellar medium *Astron. Astrophys.* **539** A32

[81] Juett A M, Schulz N S and Chakrabarty D 2004 High-resolution x-ray spectroscopy of the interstellar medium: structure at the oxygen absorption edge *Astrophys. J.* **612** 308–18

[82] Lee J C and Ravel B 2005 Determining the grain composition of the interstellar medium with high-resolution x-ray spectroscopy *Astrophys. J.* **622** 970–6

[83] Westphal A J, Butterworth A L, Tomsick J A and Gainsforth Z 2019 Measurement of the oxidation state of Fe in the ISM using x-ray absorption spectroscopy *Astrophys. J.* **872** 66

[84] Rogantini D, Costantini E, Zeegers S *et al* 2018 Investigating the interstellar dust through the Fe K-edge *Astron. Astrophys.* **609** A22

[85] Hoffman J and Draine B T 2016 Accurate modeling of x-ray extinction by interstellar grains *Astrophys. J.* **817** 139

[86] Heinz S *et al* 2015 Lord of the rings: a kinematic distance to circinus X-1 from a giant x-ray light echo *Astrophys. J.* **806** 265

[87] Heilmann R K, Kolodziejczak J, Bruccoleri A R, Gaskin J A and Schattenburg M L 2019 Demonstration of resolving power $\lambda/\delta\lambda > 10\,000$ for a space-based x-ray transmission grating spectrometer *Appl. Opt.* **58** 1223

[88] Arnaud M and Raymond J 1992 Iron ionization and recombination rates and ionization equilibrium *Astrophys. J.* **398** 394–406

[89] Culhane J L *et al* 2007 The EUV imaging spectrometer for hinode *Sol. Phys.* **243** 1